Retrieving crop fractional cover and LAI based on airborne Lidar data

CUI Yaokui[1], ZHAO Kaiguang[2], FAN Wenjie[1], XU Xiru[1]

1. *Institute of RS and GIS*, *Peking university*, *Beijing* 100871, *China*;
2. *Center on Global Change*, *Duke University*, *Durham*, *NC* 27708, *USA*

Abstract: Light detection and ranging (Lidar) point cloud data contains the information of the 3D coordinate and intensity, which can be applied to acquire the height of crown, fractional cover *etc*. in high-statue vegetation, such as the forest. Meanwhile, with the improvement of data storage capacity and processing speed, small footprint airborne Lidar is able to store the entire reflected waveform through digitally sampling, which expands the application of Lidar. However, the methods used in forest are not suitable for shrubs, crops and other low canopies. In this paper, we choose the cron as the study object, and propose a crop fractional cover and leaf area index (LAI) retrieval method using airborne Lidar intensity of ground hits and the distance and zenith angle information contained in waveforms data. Relevant fight experiment and ground measurements in Heihe indicate that the method is reliable, and the experiment also validates the great potential for Lidar to be applied to monitor low natural vegetation in agriculture.

Key words: Lidar, point cloud, full waveform, crop, fractional cover, LAI

CLC number: TP79 **Document code:** A

Citation format: Cui Y K, Zhao K G, Fan W J and Xu X R. 2011. Retrieving crop fractional cover and LAI based on airborne Lidar data. *Journal of Remote Sensing*, **15**(6): 1276–1288

1 INTRODUCTION

Vegetation canopy plays a key role in the carbon-cycle and energy transfer. Vegetation structural parameters, such as fractional cover, and leaf area index (LAI), serve as critical inputs or parameters in driving ecosystem-related models, such as biogeochemical and crop yield estimation models (Bonan, 1993; Fan & Xu, 2005; Morsdorf, *et al*., 2006), and also for the region or global climate models and monitoring the global change (Avissar & Pielke, 1989; Weiss & Baret, 1999). Crops are a typical kind of vegetation cover and it is very important to gain the fractional cover and LAI accurately for crop yield and growing monitoring.

Typically, approaches to retrieving fractional cover and LAI from optical images can be categorized into two groups, regression models (Cohen, *et al*., 2003; Colombo, *et al*., 2003) and radiative transfer models (Kotz, *et al*., 2004; Schlerf, *et al*., 2006). But both groups of retrieval models fail to work appropriately when we have to estimate these structural variables such as LAI at the high values, primarily due to the saturation of optical signals for canopies with large LAI (Morsdorf, *et al*., 2006). In contrast, the airborne laser system as an active sensor, using the objects' backscatter characteristic, can accurately acquire the 3D coordinates and echo intensity of the ground points. These information allows explicitly retrieve the fractional cover, LAI and canopy height of forest and much progress has been made recently (Andersen, *et al*., 2005; Lefsky, *et al*., 1999; Means, *et al*., 1999; Solberg, *et al*., 2009; Zhao, *et al*., 2009).

Although considerable successes have been documented in deploying Lidar to map forest ecosystems, these methods are not suitable for low-statute vegetation like croplands and grasslands. It is necessary to classify the points into ground points and vegetation points in retrieving the fractional cover and LAI. Three types of methods are often adopted in previous research on Lidar remote sensing of forests. Separating vegetation and ground echoes is based on: (1) a height threshold relative to a digital terrain model (Morsdorf, *et al*., 2006; Solberg, *et al*., 2009); (2) the echo types such as the first echo, last echo and single echo (Sasaki, *et al*., 2008); (3) the intensity information (Bao, *et al*., 2008). All the retrieval structural parameters methods are based on classifying the points, taking the point as one sampling of the ground or vegetation. However, for the low canopy vegetation such as the crops, all leaves gathered at the center, so the area of leaf is not large enough at any height. Consequently, the energy reflected by the crop will not be recorded by the sensor. Thus most of the points are reflected by the ground. For this reason retrieving fractional cover by calcu-

Received: 2010-11-17; **Accepted**: 2011-02-18

Foundation: The National Natural Science Foundation of China(No. 40734025, 40871186); The National High Technology Research and Development Program of China(863 program) (No. 2009AA12Z143); The National Basic Research Program(973 program) (No. 2007CB714402); "Watershed Allied Telemetry Experiment Research (WATER)" remote sensing experiment(No. KZCX2-XB2-09)

First author biography: CUI Yaokui (1984—), male, master candidate, majors in quantitative remote sensing. E-mail: yaokuicui@163.com

Corresponding author biography: FAN Wenjie(1972—), female, Ph.D., associate professor, her research interests are quantitative remote sensing, ecology remote sensing and thermal infrared remote sensing. She has publishied over 10 SCI papers. E-mail: fanwj@pku.edu.cn

lating the ratio of ground echo and vegetation echo will miss much vegetation information.

For small-footprint Lidar, the diameter is less than 1 m, so most pluses can penetrate through the canopy and are recorded as ground echoes by Lidar system. Moreover, sometimes there are some vegetation echoes for the dense vegetation. In the cropland, the ground echo is weakened by the vegetation before reaching the ground. Thus, the ground echo contains both vegetation information and soil information. Based on this characteristic, choosing the corn as the object, we propose a new method to acquire vegetation information and then retrieve fractional cover and LAI.

2 MATERIALS

2.1 Study site

The experimental region is the Yingke oasis located near Zhangye City, Gansu Province, in the middle reach of the Heihe River Basin (37°45′N—42°40′N, 97°42′E—102°04′E), which is the second largest inland river basin in China. The site is surrounded by mountains around valley, and mainly influenced by the climate in high-altitude cloud circulation control and polar cold air mass. Climate is dry and the precipitation is scarce but concentrated. There are many crops and forest distributed on the irrigated oasis, which is on the alluvial fan and alluvial plain in the middle Heihe river. The study area is the yingke oasis (100.411°E, 38.857°N), located in the north of Zhangye City. In the study area, main vegetation includes corn, wheat, barley, and flax, and some orchard, few roads stretching and residents living here. The landscape pattern and composition of plant communities for this region can be found at this website: [2011-02] http://heihe.westgis.ac.cn .

2.2 Lidar data

The data, used in this paper, was acquired on 2008-06-20. An airborne laser scan flight was carried out in the study area. The airborne laser scanning system (LiteMapper-5600) is developed by the German company Ingenier-Gesellschaft fur Interfaces (IGI). The laser scanner is RIEGL LMS-Q560, with laser wavelength of 1550 nm, and laser pulse length of 3.0 ns, and laser beam divergence of 0.5 mrad. Lidar point cloud data uses WGS84 coordinate system, and a universal transverse Mercator (UTM) projection with 47 belt in northern hemisphere. The flight altitude is 700 m above the ground and the footprint diameter is about 0.35 m, which is small so that the pulse can easily get through some sparse farmland and completely reach the ground. In this paper, both point cloud and full waveform data are used. For point cloud, the system records three types of echo, first echo, last echo and single echo (first echo=last echo), with point density of 0.81 points per square meter. The full waveform data contains information about the scanning angle, time interval between launch wave and reflection wave.

2.3 Field data

Four corn fields on the flight were selected as the sampling fields, and were sampled on 2008-06-21. The fractional cover was measured using a Nikon Coolpix 8400 camera. Method for LAI acquisition uses the Yao's method (Yao, *et al*., 2010). According the corn growth, we chose the corns from the other corn fields with similar growth conditions , and then measured the leaf area by LAI-3000 to determine LAI. Each sample has precise GPS positioning data. Fig. 1 is the distribution of Lidar research area and validation sample area.

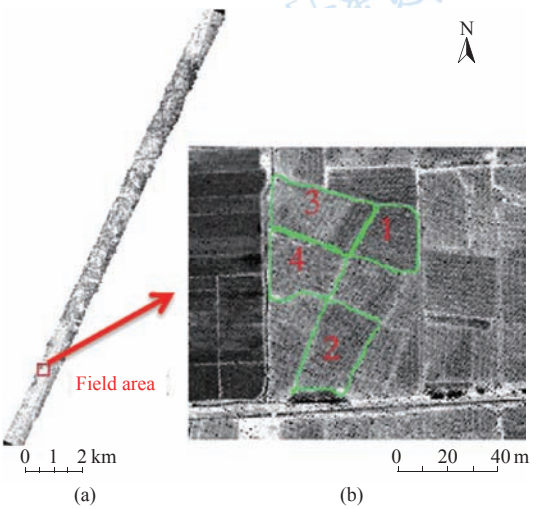

Fig. 1 Description of research area
(a) The whole research area; (b) The field area of four plots

3 PRINCIPLE AND METHOD

3.1 Theoretical background

Lidar launches a pulse in a short time. When meeting obstacles, the pluse will return. If the return energy is larger than the threshold of the system, the system will record it as one point, including 3D and intensity information.

Point cloud intensity is influenced by many factors, such as reflectance of the target, target-sensor distance, scanning zenith angle, and atmospheric condition (Donoghue, *et al*., 2007). Nevertheless, when the points are gained by the same flight, the moisture content and roughness of soil, and even the atmospheric condition are very similar.

According to Wagner, the received energy can be specified by the Eq. (1) (Bao, *et al*., 2008; Wagner, *et al*., 2006)

$$P_r = \frac{P_t D_r^2 \rho}{4\pi R^4 \beta_t^2} \eta_{sys} \eta_{atm} A_s \quad (1)$$

where P_r and P_t are the received and transmitted laser energy respectively, R the sensor-target distance, β_t the laser-beam divergence, D_t the diameter of the receiver aperture, ρ the reflectance of the target surface, $\eta_{sys}$and η_{atm} the system and atmospheric transmission factors, respectively, and A_s the illuminated target area.

Laser pulse can penetrate vegetation and reach the ground. At the same time, the system records different echoes according to the return time (Sui & Zhang, 2006). As a distance between ground and crop, the ground echoes recorded by the system will not contain vegetation information. If a laser pulse hits on the bare ground, its echo will be reflected entirely from the ground for the full footprint. In such a case, the target area equalizes the footprint size. In vegetation coverage area such as croplands, for a pulse, a part of the footprint is intercepted by vegetative components such as leaves and stems before the pulse reaches the ground. Therefore, only the remaining part of the footprint is able to arrive at the ground without being collided. Let A_{max} be the illuminated area of non-

vegetated ground and P_{max} the corresponding received energy. Let A_g be the ground area illuminated directly by the laser pulse through a vegetation layer and P_g the received energy for the corresponding ground echo. Then

$$\frac{P_g}{P_{max}} = \frac{\frac{P_t D_r^2 \rho}{4\pi R_g^4 \beta_t^2}\eta_{sys}\eta_{atm}}{\frac{P_t D_r^2 \rho}{4\pi R_{max}^4 \beta_t^2}\eta_{sys}\eta_{atm}} \times \frac{A_g}{A_{max}} \tag{2}$$

In the study area, the variability of ρ can be very low, because the angle on non-principal plane is less than 30°, according to the field measured BRDF. Furthermore, P_t, D_r, β_t, η_{sys} and η_{atm} are only affected by the system and scanning environment, and the variability of these parameters is low enough during one flight. Meanwhile, R can be acquired from full waveform data.

$$\frac{A_g}{A_{max}} \approx \frac{P_g \times R_g^4}{P_{max} \times R_{max}^4} \tag{3}$$

The left side of Eq. (3) is the gap fraction (f'_{gap}) for a pulse sampling.

The value of intensity and the received energy has a linear relationship (Langford, *et al*., 2006), so

$$f'_{gap} = \frac{A_g}{A_{max}} \approx \frac{I_g \times R_g^4}{I_{max} \times R_{max}^4} \tag{4}$$

where I_g and I_{max} represent the intensity, corresponding with A_g and A_{max}, respectively.

We divided the study area into 5 m × 5 m grids, where there may be a number of (n) ground echoes, and the gap fraction f_{gap} for one grid then can be approximated by

$$f_{gap} = \frac{1}{n}\sum_{j=1}^{n} f'_{gapj} \approx \frac{1}{n}\sum_{j=1}^{n} \frac{I_{gj} \times R_{gj}^4}{I_{max} \times R_{max}^4} \tag{5}$$

where n is the count of points in one grid, f'_{gapj}, I_{gj} and R_{gj} are the gap fraction, the intensity and the sensor-target distance of the j^{th} ground echo, respectively.

3.2 Full waveform

The attributes of each Lidar pulse are stored in a file, suffixed for ".LGC" (Li & Ma, 2008). From the file, the sensor-target distance (R), scanning zenith angle (θ) can be calculated by the following equation.

$$R = WFOFFSET \times d \tag{6}$$

$$\theta = \arccos\left(\frac{-dH}{\sqrt{dE^2 + dN^2 + dH^2}}\right) \tag{7}$$

WFOFFSET is the time offset between the launch pluse and the return pluse, d is the sampling distance with a value of 0.149855 m. dE, dN, dH are the differential of the sampling units, and dH is a negative value.

3.3 Calculation of gap fraction

Calculating gap fraction using Eq. (4) and Eq. (5) requires ground echoes, which should be separated from vegetation echoes firstly and conducted using a professional software. TerraSolid is a product dealing with the Lidar data of Finland TerraSolid company, running at Microstation SE/JTM platform. TerraScan, one of TerraSolid software, can read and deal with the Lidar point cloud, and classify the points according to the coordinate, intensity *etc.*, ensures to separate the ground points from the vegetation points (Zhang, *et al*., 2009).

In this paper, the ground points in the corn field are extracted, using the digital surface model (DSM) and digital elevation model (DEM) method (He, *et al*., 2009) and the classification results of visible image.

(1) Generating DEM: TerraScan offers the function model for classifying the ground points. The algorithm principle firstly chooses some low points, according to the area of max building to serve them as land surface points. And then, it repeatedly builds the triangle-net to gain the ground points (Guan & Li, 2009). After gaining the ground points, it uses the TerraScan software to generate and interpolate the ground points into 1 m resolution DEM.

(2) Generating the DSM: transforming the point cloud into grid, when there have multiple points, using the max value as the pixel value. When the pixel value equals to 0, using the average value around the pixel interpolates the grid data. And then getting 1 m resolution DSM.

(3) Separating the cropland: generating the canopy height model (CHM) by DSM minus DEM. For a 3×3 window, if the central pixel is the minimum, let the pixel value equal to the average of the window. Furthermore, according to prior knowledge, if the CHM is less than 2.5 m, the points in the grid are the crop points. And then, we can get the Lidar points in the cropland.

(4) Gaining the points in the corn field: generating the corn classification with an accuracy of 90%, using 10 m resolution SPOT 5 image (2008-07-04), by the maximum likelihood method. According to the longitude and latitude of the classification results, the Lidar points in the corn field can be extracted.

(5) Gaining the ground points in the corn field: using the TerraScan to extract the ground points in the corn field.

(6) Calculating the value of $I_{max} \times R_{max}^4$ for every point. According to the longitude and latitude, the indensity I and sensor-target distance R of every point can be gained. As usual, the points in the middle of the classification results can be considered as the pure pixels, considering the maximum likelihood classification's accuracy and features. For the huge number of points, we choose the first one hundred points according to the value of $I_{max} \times R_{max}^4$ by size, and then use the average as the $I_{max} \times R_{max}^4$ value. We use the average of these one hundred points as the value $I_{max} \times R_{max}^4$ of pure pixel. At last, we calculate the gap fraction for the whole flight line, by the Eq. (4) and Eq. (5) .

3.4 Retrieval of fractional cover

After gap fraction calculated, the fractional cover is computed from Eq. (8) as

$$f_{cover} = 1 - f_{gap} \tag{8}$$

3.5 Retrieval of LAI

The probability of photons directly reaching the ground represents canopy transmittance:

$$T_0 = e^{-\lambda_0 \cdot \frac{G}{\mu} \cdot LAI} \tag{9}$$

where λ_0 is the Nilson parameter considering vegetation clumping effect, G is the mean projection of a unit of leaf area into the

plane perpendicular to the incident laser direction, μ is the cosine of the zenith angle. Canopy transmittance (T_0) equals to the gap fraction (f_{gap}).

$$f_{gap} = e^{-\lambda_0 \frac{G}{\mu} \mathrm{LAI}} \tag{10}$$

where μ can be calculated by the scanning angle. G and λ_0 can be inferred from the prior knowledge. Accordingly, LAI can be calculated by simply inverting Eq. (11)

$$\mathrm{LAI} = -\frac{\ln(f_{gap})}{\lambda_0 \cdot G}\mu \tag{11}$$

4 RESULT AND ANALYSIS

4.1 Retrieval of fractional cover

According to the methods above, retrieve the fractional cover of corn by the 5 m×5 m grid (Fig. 2)

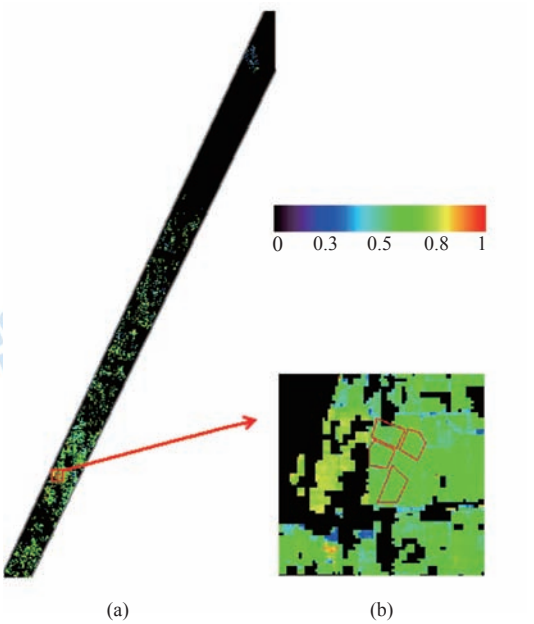

Fig. 2 Retrieval results of corn fractional cover derived from Lidar data
(a) The whole research area; (b) The field area of four plots

Calculate the average fractional cover for each plot. Table 1 is the fractional cover retrieved from Lidar data and field data. Fig. 3 is the statistical result of the whole research area (the whole flight), and the black line in the figure represents the distribution of the validation data.

Table 1 Comparisons of fractional cover between those derived from Lidar and field measurements for the four corn fields

Plots	Lidar results		Field measurements		Absolute error	Relative error/%
	Average	Standard deviation	Average	Standard deviation		
1	0.651	0.024	0.654	0.049	0.003	0.459
2	0.630	0.030	0.625	0.000	0.005	0.800
3	0.589	0.038	0.600	0.012	0.011	1.833
4	0.573	0.018	0.515	0.035	0.058	11.262

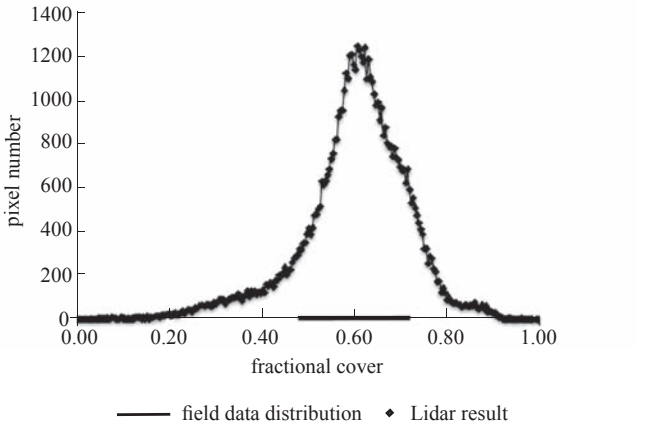

Fig. 3 Fractional cover statistical results of the whole study area

From Table 1, it is clear that the fractional cover of Lidar and filed data agree well, and only the 4th plot has a relative large error. The reason is that the tiny difference of soil condition and the scanning angle, may cause different soil BRDF, resulting in the retrieval error.

In Fig. 3, there are more than 80% retrieval result points distributing in the range of field data. That is because the similar growth conditions for the same crop in the same region. The unusual values maybe caused by classification results. Actually, the fractional cover maybe zero for the roads, and in contra the fractional cover is larger than corn for wheat and orchard.

4.2 Retrieval of LAI

Corn leaf shows a sphere distribution, so G=0.5 can be used as the prior knowledge. Meanwhile, λ_0 dependents on the scanning angle, width of the row, distance of the two rows, canopy height and LAI. In this paper, calculate λ_0 under different view angles According to the field structural parameters of corn (Yan, *et al*., 2010), as Fig. 4. According to the gap fraction, the scanning angle and λ_0, the plots LAI can be retrieved by Eq. (11). For the four plots, the average of each pixel LAI is the plot LAI, as Fig. 5. Table 2 is the LAI retrieved from Lidar data and field data. Fig. 6 is the statistical result of the whole research area (the whole flight), and the black line in the figure represents the distribution of the field data.

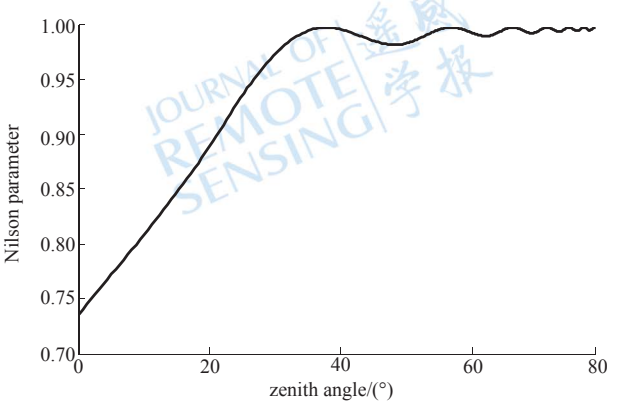

Fig. 4 The relationship between Nilson parameter and view zenith angle

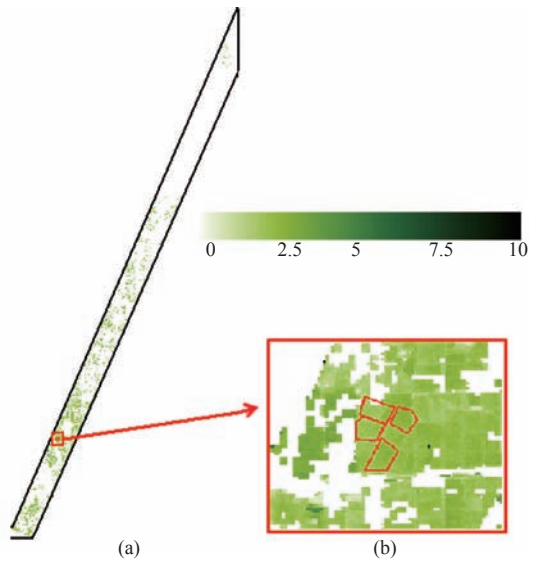

Fig. 5 Retrieval results of corn LAI derived from Lidar data
(a) The whole research area; (b) The field area of four plots

Table 2 Comparisons of LAI between those derived from Lidar and field measurements for the four corn fields

Plots	Lidar results		Field measurements		Absolute error	Relative error /%
	Average	Standard deviation	Average	Standard deviation		
1	2.49	0.25	2.295	0.518	0.195	8.5
2	2.34	0.24	2.04	0.249	0.3	14.7
3	1.92	0.68	1.98	0.345	0.06	3
4	2.15	0.21	2.3	0	0.15	6.5

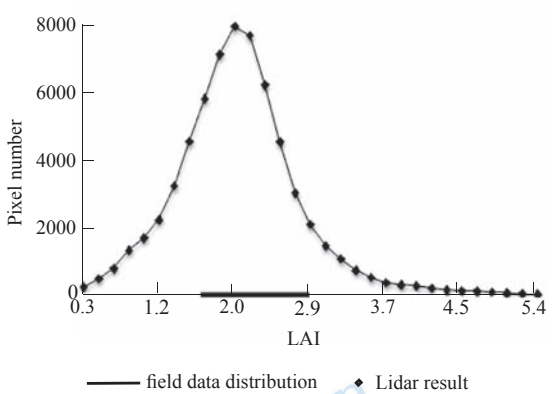

Fig. 6 LAI statistical result of the whole study area

From Table 2, it is clear that the LAI of Lidar and filed data agree well, and only that the 2th plot has a relative large error. There are two reasons for the error, including fractional cover and λ_0. The retrieval error of fractional cover will transfer to LAI. Meanwhile, many factors will affect λ_0, such as G, width of the row, distance of the two rows, canopy height, LAI and the height of flight. In this paper, λ_0 is determined by the field data, which only reduces the error for different scanning angle. So the error may not be avoidable for λ_0. Actually, as shown in Fig. 4, for row crop, view angle is one of the important influence factors for λ_0. When other factors are equal, the λ_0 considering the view angle is more close to the real λ_0. Compared with using λ_0 as a fixed value traditionally which completely without consider the influence of angle for λ_0, the method used in this paper can give better LAI estimates.

In Fig. 6, there are more than 80% retrieval points distributing in the range of field data, for LAI. Apart from the classification error, the distribution is reasonable with the corn growth.

5 CONCLUSION

In this study, the mechanism of airborne Lidar scanning was analyzed, and the Lidar point cloud and full waveform data were used to retrieve the fractional cover and LAI in cropland. According to equation, the gap fraction is gained from the intensity information of ground echoes. Then the fractional cover and LAI of the whole flight line were retrieved. Field validation shows that the method can accurately retrieve these parameters of crop fields.

Classifying the Lidar point cloud is a difficult issue. And meanwhile, when get the pure ground echoes of the corn field, we need a higher accuracy of classification. In this paper, firstly using the method of DSM and DEM to get the canopy heigh model, and after that, filter the points using the visible image classification. Finally, Lidar points in corn field are extracted.

In this paper, we choosed corn field as study objects to retrieve fractional cover and LAI. Meanwhile, the method is proposed for the low canopy vegetation. Results show that retrieving fractional cover and LAI with high accuracy and resolution is possible using the Lidar data. In the future, Lidar will have extensive applications for precision agriculture and other agricultural production.

REFERENCES

Andersen H E, McGaughey R J and Reutebuch S E. 2005. Estimating forest canopy fuel parameters using LiDAR data. *Remote Sensing of Environment*, **94**(4): 441–449

Avissar R and Pielke R A. 1989. A parameterization of heterogeneous land surfaces for atmospheric numerical models and its impact on regional meteorology. *Monthly Weather Review*, **117**(10): 2113–2136 DOI: 10.1175/1520–0493(1989)117<2113:APOHLS>2.0.CO;2

Bao Y F, Cao C X, Zhang H, Chen E X, He Q S, Huang H B, Li Z Y, Li XW and Gong P. 2008. Synchronous estimation of DTM and fractional vegetation cover in forested area from airborne LIDAR height and intensity data. *Science in China Series E-Technological Sciences*, **51**(Suppl. 2): 176–187

Bonan G B. 1993. Importance of leaf area index and forest type when estimating photosynthesis in boreal forests. *Remote Sensing of Environment*, **43**(3): 303–314

Cohen W B, Maiersperger T K, Gower S T and Turner D P. 2003. An improved strategy for regression of biophysical variables and Landsat ETM+data. *Remote Sensing of Environment*, **84**(4): 561–571

Colombo R, Bellingeri D, Fasolini D and Marino C M. 2003. Retrieval of leaf area index in different vegetation types using high resolution satellite data. *Remote Sensing of Environment*, **86**(1): 120–131

Donoghue D N M, Watt P J, Cox N J and Wilson J. 2007. Remote sensing of species mixtures in conifer Remote sensing of species mixtures in conifer plantations using LiDAR height and intensity data. *Remote Sensing of Environment*, **110**(4): 509–522

DOI: 10.1016/j.rse.2007.02.032

Fan W J and Xu X R. 2005. Integrative inversion of land surface component temperature. *Science in China Series D-Earth Sciences*, **48**(11): 2011–2019

Guan F X and Li F W. 2009. Research on features extraction based on LiDAR. *Geomatics and Spatial Infromation Technology*, **32**(1): 134–135, 140

He Q S, Chen E X, Cao C X, Liu Q W and Pang Y. 2009. A study of Forest Parameters Mapping Technique using Airborne LIDAR Data. *Advances in Earth Science*, **24**(7): 748–755

Kotz B, Schaepman M, Morsdorf F, Bowyer P, Itten K and Allgower B. 2004. Radiative transfer modeling within a heterogeneous canopy for estimation of forest fire fuel properties. *Remote Sensing of Environment*, **92**(3): 332–344

Langford J, Niemann O, Frazer G, Wulder M A and Nelson T. 2006. Exploring small footprint Lidar intensity data in a forested environment//*Proceedings*, *IEEE International Conference on Geoscience and Remote Sensing Symposium*. Denver: IEEE: 2416—2419

Lefsky M A, Cohen W B, Acker S A, Parker G G, Spies T A and Harding D. 1999. LiDAR remote sensing of the canopy structure and biophysical properties of Douglas-fir western hemlock forests. *Remote Sensing of Environment*, **70**(3): 339–361

Li Q and Ma H C. 2008. The study of Point-cloud Production Method based on Waveform Laser Scanner Data. *Acta Geodaetica et Cartographica Sinica*, **37**(3): 349–354

Means J E, Acker S A, Harding D J, Blair J B, Lefsky M A, Cohen W B, Harmon M E and McKee W A. 1999. Use of large-footprint scanning airborne lidar to estimate forest stand characteristics in the Western Cascades of Oregon. *Remote Sensing of Environment*, **67**(3): 298–308

Morsdorf F, Kötz B, Meier E, Itten K I and Allgöwer B. 2006. Estimation of LAI and fractional cover from small footprint airborne laser scanning data based on gap fraction. *Remote Sensing of Environment*, **104**(1): 50–61 DOI: 10.1016/j.rse.2006.04.019

Sasaki T, Imanishi J, Ioki K, Morimoto Y and Kitada K. 2008. Estimation of leaf area index and canopy openness in broad-leaved forest using an airborne laser scanner in comparison with high-resolution near-infrared digital photography. *Landscape and Ecological Engineering*, **4**(1): 47–55 DOI: 10.1007/s11355-008-0041-8

Schlerf M and Atzberger C. 2006. Inversion of a forest reflectance model to estimate structural canopy variables from hyperspectral remote sensing data. *Remote Sensing of Environment*, **100**(3): 281–294

Solberg S, Brunner A, Hanssen K H, Lange H, Naesset E, Rautiainen M and Stenberg P. 2009. Mapping LAI in a Norway spruce forest using airborne laser scanning. *Remote Sensing of Environment*, **113**(11): 2317–23271 DOI: 10.1016/j.rse.2009.06.010

Sui L C and Zhang B Y. 2006. Principle and trend of Airborne Laser Scanning Remote Sensing. *Journal of Zhengzhou Institute of Surveying and Mapping*, **23**(2): 127–129

Wagner W, Ullrich A, Ducic V, Melzer T and Studnicka N. 2006. Gaussian decomposition and calibration of a novel small-footprint full-waveform digitising airborne laser scanner. *ISPRS Journal of Photogrammetry and Remote Sensing*, **60**(2): 100–112 DOI: 10.1016/j.isprsjprs.2005.12.001

Weiss M and Baret F. 1999. Evaluation of canopy biophysical variable retrieval performances from the accumulation of large swath satellite data. *Remote Sensing of Environment*, **70**(3): 293–306 DOI: 10.1016/S0034-4257(99)00045-0

Yan B Y, Xu X R and Fan W J. 2010. A unified canopy bidirectional reflectance(BRDF) model for row crops. *Science in Chnia Series D*, Accepted

Yao Y J, Fan W J, Liu Q, Li L, Tao X, Xin X Z and Liu Q H. 2010. Improved harvesting method for corn LAI measurement in corn whole growth stages. *Transactions of the CSAE*, **26**(8): 189–194

Zhao K G and Popescu S. 2009. LiDAR-based mapping of leaf area index and its use for validating GLOBCARBON satellite LAI product in a temperate forest of the southern USA. *Remote Sensing of Environment*, **113**(8): 1628–1645

Zhang J, Zhang X Y and Cao H C. 2009. Post-processing of Airborne LiDAR Data based on Terrasolid Software. *Sci-Tech Information Development and Economy*, **19**(26): 90–92

机载Lidar数据的农作物覆盖度及LAI反演

崔要奎[1]，赵开广[2]，范闻捷[1]，徐希孺[1]

1. 北京大学 遥感与地理信息系统研究所，北京 100871;
2. 达勒姆市杜克大学 全球变化中心，北卡罗来纳州， 27708

摘 要：虽然Lidar点云数据已被广泛应用于获取森林各项结构参数，但这些方法并不适合于低矮的灌丛、林地和农作物。本文以玉米为研究对象，提出利用机载Lidar点云数据的强度信息和全波形数据中的距离与扫描天顶角信息，反演农作物覆盖度和LAI的方法。在黑河进行的飞行实验和地面验证表明，该方法具有较高精度，也表明Lidar在低矮自然植被监测和农业应用上有较大潜力。

关键词：Lidar，点云，全波形，农作物，覆盖度，LAI

中图分类号：TP79 **文献标志码**：A

引用格式：崔要奎，赵开广，范闻捷，徐希孺. 2011. 机载Lidar数据的农作物覆盖度及LAI反演. 遥感学报，**15**(6): 1276–1288
Cui Y K, Zhao K G, Fan W J and Xu X R. 2011. Retrieving crop fractional cover and LAI based on airborne Lidar data. *Journal of Remote Sensing*, **15**(6):1276–1288

1 引 言

植被冠层在碳循环和能量传输中起着重要作用，植被覆盖度、叶面积指数(LAI)作为植被冠层的结构参数，是很多关于能量、生物量等反演模型的重要输入参数(Bonan，1993；Fan和Xu，2005；Morsdorf 等，2006)，也是区域、全球气候模型以及全球变化监测必需的输入参数之一(Avissar和Pielke，1989；Weiss和Baret，1999)。农作物作为典型的地表植被覆盖类型，准确地获取其覆盖度和LAI是精确估算作物产量及进行长势监测的必要条件。

利用光学影像反演覆盖度及LAI主要有两种方法：一种是基于回归模型(Cohen 等，2003；Colombo 等，2003)，另一种是基于辐射传输模型(Kotz 等， 2004; Schlerf和Atzberger，2006)。但是光学信号在叶面积指数较大时容易饱和，并受大气等因素的影响，这些方法的应用有一定限制(Morsdorf 等，2006)。机载激光雷达作为一种主动式传感器，根据地物后向散射特性，能高精度地获取地面点三维坐标和回波强度信息，为监测植被生长状态提供了新的技术手段，并已经在反演森林的覆盖度、LAI、株高及冠层高度等方面(Andersen 等，2005； Lefsky 等，1999； Means 等，1999； Solberg 等, 2009； Zhao和Popescu，2009)取得了很大进展。

虽然Lidar在获取森林结构参数方面已取得很多成果，但是这些反演方法并不适用于农作物等低矮植被的结构参数反演。分类植被点和地面点是反演覆盖度和LAI的必要前提，在森林研究中，研究者通常用3种方法来实现植被点和地面点的分离：(1)先建立地面模型，然后设定一高程阈值，进行植被点和地面点分离(Morsdorf 等，2006；Solberg 等，2009)；(2)根据首次回波、末次回波及仅有一次回波的这些回波类型简单地进行植被和地面点分类(Sasaki 等, 2008)；(3)利用强度信息实现地面和植被点的分离(Bao 等，

收稿日期：2010-11-17；**修订日期**：2011-02-18

基金项目：国家自然科学基金(编号: 40734025, 40871186)；国家高技术研究发展计划(863计划) (编号: 2009AA12Z143)；国家重点基础研究发展计划(973计划) (编号: 2007CB714402)；中国科学院西部行动计划(二期)项目“黑河流域遥感—地面观测同步试验与综合模拟平台建设”(编号: KZCX2-XB2-09)

第一作者简介：崔要奎(1984—)，男，硕士研究生，研究方向为定量遥感。E-mail: yaokuicui@163.com。

通信作者简介：范闻捷(1972—)，女，博士，副教授，研究方向为定量遥感、生态遥感和热红外遥感，已发表SCI论文10余篇，EI、核心刊物论文20余篇。E-mail:fanwj@pku.edu.cn。

2008)。以植被点和地面点分离为基础的结构参数反演方法，都把任意一个地面点看做是对地面或植被的一次采样。对农作物等低矮植被而言，不但个体比较矮小，而且其叶片聚集方式多是以株为中心的，因此在任一高度上其叶片的比例并不大，这样在形成回波时很难形成较高的反射能量，以至于Lidar传感器无法记录，因此传感器记录的大部分点均来自于地面。因此，这种把回波点看作完全是地面或植被的采样，并以此为根据把Lidar回波点分为植被和土壤两类，继而通过计算二者的比率来计算农作物覆盖度的方法，会造成很多植被信息的丢失。

小光斑Lidar到达地面的光斑直径一般在1 m以下，大部分的Lidar光斑都可以穿过植被冠层，到达地面而形成地面回波，也有一些点仅由植被反射而形成。在农作物覆盖区，这些地面回波点是先经过植被削弱后到达地面而形成的，因而里面既有植被信息又有土壤信息。本文根据这一特点，利用机载激光雷达的离散点云数据和全波形数据，以与人类生活息息相关的低矮农作物—玉米为主要研究对象，结合雷达方程进行分析，利用Lidar的强度信息和全波型数据中的距离及扫描角度信息，从地面回波中提取植被信息，进而求取覆盖度和LAI。实验验证表明此方法切实可行。

2 数 据

2.1 试验区概况

选择中国第二大内陆河流域黑河流域中部的张掖盈科灌区为试验区，黑河流域(37° 45′ N—42° 40′ N, 97° 42′ E—102° 04′ E)位于河西走廊中部，是中国西北地区第二大内陆流域，远离海洋，周围高山环绕，流域气候主要受中高纬度的西风带环流控制和极地冷气团影响，气候干燥，降水稀少而集中。中游山前冲积扇下部和河流冲积平原上分布有灌溉绿洲栽培农作物和林木。研究区为分布在中游绿洲区的甘肃省张掖市境内的盈科灌溉区，地理坐标为(100.411° E, 38.857° N)，北部为张掖市城区，南部为地势平坦的农田，研究区再往南是戈壁，主要植被以农作物(如玉米、小麦、大麦和胡麻等)为主，还有少量的果园，道路与居民地零散地分布其间。具体的研究区景观分类、主要植被群落及其分布请参考：[2011-02] http://heihe.westgis.ac.cn。

2.2 Lidar数据

本文机载Lidar数据获取时间为2008-06-20，飞行区域为张掖试验区盈科气象站附近，采用的Lidar系统为LiteMapper 5600，其中激光扫描仪为Riegl LMS-Q560，波长1550 nm，激光脉冲长度3.0 ns，激光脉冲发散角小于等于0.5 mrad。Lidar点云数据采用WGS84坐标系，UTM投影北半球6° 分带的第47带。飞机飞行相对航高约700 m，到达地面的光斑直径约0.35 m，这个光斑直径很小，很容易穿过某些稀疏的农田间隙而完全到达地面。所用Lidar数据包括离散点云数据和全波形数据，对于离散点云数据系统记录了首次回波、末次回波及仅有一次回波的点，平均点密度为0.81个/m^2，而全波形数据记录了扫描角、发射波与反射回波时间间隔等参数。

2.3 验证数据

在航带上共选取4块玉米样地，作为验证数据的样区。验证数据获取时间是2008-06-21，利用Niken Coolpix 8400相机测量样地覆盖度，叶面积指数测量采用姚延娟等人的方法(姚延娟 等，2010)，根据每块样地的长势，选取其他地块能代表这一长势的若干株玉米，用LAI-3000测量叶面积，然后计算叶面积指数，每块样地都有精确的GPS定位，图1是Lidar研究区与验证样区的分布情况。

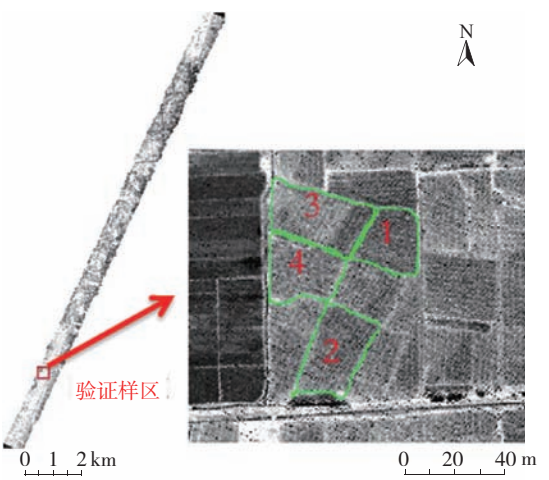

(a) (b)

图1 试验区影像

(a) 整个研究区；(b) 验证区的4块玉米样地

3 原理与方法

3.1 理论与背景

Lidar是在非常短的时间内发射一个脉冲，这些脉冲遇到障碍物便返回，并记录能量值大于系统可以记录阈值的点，记录信息包括空间三维位置信息和强度信息，这就形成了离散点云数据。

Lidar回波强度受各种因素的影响，包括地物反射率、粗糙度、传感器与目标的距离、观测视角、甚至大气状况等(Donoghue 等，2007)。尽管影响因素很多，但研究区处于同一个航带，农田土壤的含水量、粗糙度及天气状况等基本相同。

根据Wagner等人的推导(Bao 等，2008; Wagner 等，2006)，激光发射至地面物体并反射回接收器的能量如式(1)：

$$P_r = \frac{P_t D_r^2 \rho}{4\pi R^4 \beta_t^2} \eta_{sys} \eta_{atm} A_s \tag{1}$$

式中，P_r为接收到的能量，P_t为激光器发射的能量，R为传感器到目标的距离，β_t为发射脉冲的脉冲宽度，D_r为接收器探头的直径，ρ是目标的反射率，η_{sys}和η_{atm}为系统和大气的透过率因子，A_s是地物的反射面积。

Lidar光斑具有穿透性，同时系统根据回波时间的差异来记录不同部分的回波(隋立春和张宝印, 2006)，由于农作物和地面的高度差较大，系统记录的来自地面的回波中植被基本对回波能量没有贡献。假设一个光斑完全由农田中的裸地反射，光斑面积为A_{max}，传感器接收到的能量为P_{max}；植被覆盖区，另一光斑经过植被削减后到达地面，然后由地面反射回来，地面反射的光斑面积为A_g，传感器接收到的能量P_g。则

$$\frac{P_g}{P_{max}} = \frac{\dfrac{P_t D_r^2 \rho}{4\pi R_g^4 \beta_t^2} \eta_{sys} \eta_{atm}}{\dfrac{P_t D_r^2 \rho}{4\pi R_{max}^4 \beta_t^2} \eta_{sys} \eta_{atm}} \times \frac{A_g}{A_{max}} \tag{2}$$

在研究区，根据实测的土壤BRDF，当波长为1550 nm时，在非主平面方向土壤的反射率ρ在30° 以内变化很小，可以认为近似相等。另外激光器发射的能量P_t、脉冲宽度β_t、接收器探头直径D_r、两个透过率因子η_{sys}和η_{atm}仅与系统和当时的扫描环境有关，在一次飞行中，可以认为是不变量，每个点的距离R可由全波形数据获取。所以

$$\frac{A_g}{A_{max}} \approx \frac{P_g \times R_g^4}{P_{max} \times R_{max}^4} \tag{3}$$

式(3)左边就是一次脉冲采样获取的孔隙率(f'_{gap})。

系统记录的回波强度是反射能量的线性量化值(Langford 等，2006)，所以：

$$f'_{gap} = \frac{A_g}{A_{max}} \approx \frac{I_g \times R_g^4}{I_{max} \times R_{max}^4} \tag{4}$$

式中，I_g是A_g对应的回波强度值，I_{max}是A_{max}对应的回波强度值。

将试验区划分成5 m × 5 m大小的子样区，通过对子样区内所有地面点求孔隙率，再求平均，进而获取子样区的孔隙率。子样区孔隙率计算公式为

$$f_{gap} = \frac{1}{n}\sum_{j=1}^{n} f'_{gap_j} \approx \frac{1}{n}\sum_{j=1}^{n} \frac{I_{g_j} \times R_{g_j}^4}{I_{max} \times R_{max}^4} \tag{5}$$

式中，n代表子样区内激光点个数，f'_{gapj}代表子样区内第j个地面回波计算的孔隙率，I_{gj}代表第j个地面回波点的强度值，R_{gj}代表第j个地面回波点到传感器的距离。

3.2 全波形数据

RIEGL全波形数据文件中的*.LGC文件，记录了每一束激光的波形数据的属性(李奇和马洪超，2008)，可从中获取地面回波点与传感器的距离(R)、扫描时的入射天顶角(θ)。计算公式如下：

$$R = WFOFFSET \times d \tag{6}$$

$$\theta = \arccos\left(\frac{-dH}{\sqrt{dE^2 + dN^2 + dH^2}}\right) \tag{7}$$

*WFOFFSET*为发射脉冲的第一次采样到返回脉冲第一次采样的时间偏移量。d为采样间隔距离，为0.149855 m。dE，dN，dH是波形采样单元的坐标微分，其中dH为负值。

3.3 计算孔隙率

由式(4)和式(5)可知，孔隙率可从地面回波点中获取。因此，从Lidar数据中分离出玉米地的地面点是反演孔隙率的必要前提。由于Lidar的数据量非常巨大，通常需要专业软件来处理。TerraSolid系列软件是由芬兰TerraSolid公司出品，应用于Microstation SE/JTM平台的专业Lidar数据处理软件，其中的TerraScan软件能装载和处理大量的Lidar数据，并根据点的坐标和回波强度等信息将大量激光扫描测量数据进行分类，可以从Lidar点云数据中分离出地面点和植被点(张娟 等，2009)。

本文利用DSM和DEM的方法(何祺胜 等，2009)，结合可见光的分类结果来提取玉米地的地面点。处理过程如下：

(1)生成数字高程模型DEM(Digital Elevation Mode)：TerraScan软件提供有分类地面点的功能模块。算法原理是：先通过所分类区域最大建筑物的面积来控制选取一些低点，认为它们位于地表处；然后，通过反复建立地表三角网模型的方式分离出地面上的点(关辅兴和李芳伟，2009)。可以在TerraScan软件的支持下，分离出地面点，将地面点插值成1 m分辨率的DEM；

(2)生成数字表面模型DSM(Digital Surface Model)：首先将点云数据栅格化，当栅格单元内有多个回波点时，取其最大值作为像元值；栅格数据内插，根据0值像元的非0邻域像元进行内插，取其平均值作为内插值，根据点云密度，将DSM 插值成1 m的分辨率；

(3)分离农田：将DSM与DEM作差值处理得到冠层高度模型。对冠层高度模型进行平滑处理，平滑算法使用3 × 3窗口搜索局部最小值，使用邻域像元的平均值填充局部最小值。根据经验设定阈值，冠层高度小于2.5 m的为农作物。最后分割获取得到农田的Lidar点；

(4)提取玉米地点云数据：利用2008-07-04的SPOT 5图像，分辨率为10 m，利用最大似然法分类，得到玉米分布图，分类精度大于90%。根据分类结果的玉米地经纬度坐标截取由步骤(3)提取的农田的Lidar点，进而获取玉米地的Lidar点云数据；

(5)提取玉米地面点：在TerraScan软件的支持下，分离出玉米地面点；

(6)根据经纬度配准Lidar点云数据和从全波形数据中提取的距离信息，计算$I_{\max} \times R_{\max}^4$。考虑到可见光图像最大似然法分类的特点和分类精度，分类结果边缘的像元大都是非纯像元，而把分类结果内部的像元认为是纯像元是合理的，这样基本可以保证选取的纯裸土Lidar点来自于玉米地。同时全航带的玉米点云数据达10^5数量级，为降低偶然误差对结果的影响，取前100个$I_{\max} \times R_{\max}^4$值最大的点的平均值作为纯裸土的$I_{\max} \times R_{\max}^4$值，进而利用式(4)(5)反演全航带玉米孔隙率。

3.4 反演覆盖度

通过3.3节方法获取孔隙率以后，玉米覆盖度f_{cover}可由式(8)计算：

$$f_{\text{cover}} = 1 - f_{\text{gap}} \tag{8}$$

3.5 反演LAI

光子直接穿过冠层到达土壤的概率为冠层的透过率T_0，

$$T_0 = \mathrm{e}^{-\lambda_0 \cdot \frac{G}{\mu} \cdot \mathrm{LAI}} \tag{9}$$

式中，λ_0为考虑植被群聚效应的尼尔逊(Nilson)参数，G为单位面积内所有叶子在与太阳入射垂直平面的平均投影面积，μ为太阳天顶角的余弦，LAI为植被的叶面积指数。冠层的透过率等于孔隙率。所以

$$f_{\text{gap}} = \mathrm{e}^{-\lambda_0 \cdot \frac{G}{\mu} \cdot \mathrm{LAI}} \tag{10}$$

式中，μ可由激光扫描时的入射天顶角计算，玉米的λ_0和G可以作为先验知识获取。因此，LAI可以通过式(11)计算：

$$\mathrm{LAI} = -\frac{\ln(f_{\text{gap}})}{\lambda_0 \cdot G}\mu \tag{11}$$

4 结果与分析

4.1 反演覆盖度

根据3.1节—3.4节所述方法，以5 m × 5 m大小格网划分子样区，反演玉米覆盖度，结果如图2。

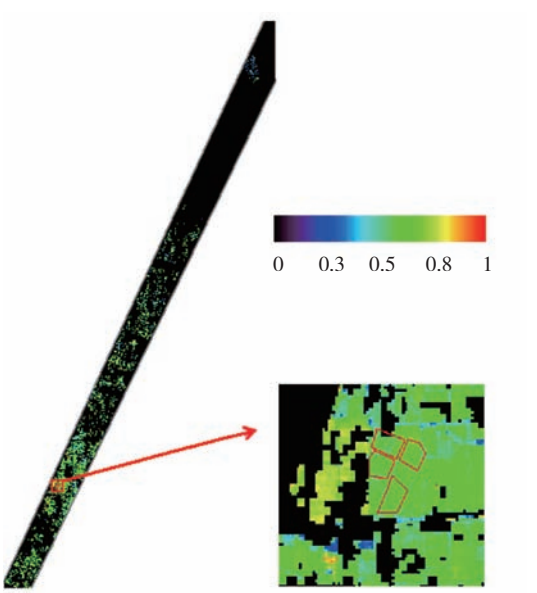

(a) (b)

图2 Lidar反演的玉米覆盖度

(a) 整个研究区；(b) 验证区的四块样地

对验证区4块样地的所有子样区进行统计，求平均值，获得每块样地的平均覆盖度。表1是Lidar反演的玉米覆盖度与实测的覆盖度的比较，图3是整个研究区(整条航带)覆盖度反演结果的统计，图中的黑线表示实测覆盖度的分布范围。

表1 玉米覆盖度反演值与实测值的比较

样地编号	Lidar反演结果		实测结果		绝对误差	相对误差/%
	均值	标准差	均值	标准差		
1	0.651	0.024	0.654	0.049	0.003	0.459
2	0.630	0.030	0.625	0.000	0.005	0.800
3	0.589	0.038	0.600	0.012	0.011	1.833
4	0.573	0.018	0.515	0.035	0.058	11.262

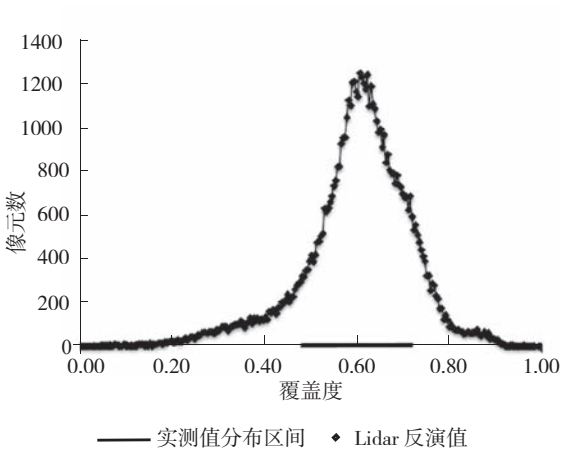

图3 整个研究区覆盖度反演结果统计

从表1可以看出，Lidar覆盖度反演结果与实测的覆盖度值相比总体上很接近，只有第4块地误差较大。反演误差产生的原因，是对土壤反射率相等的近似，土质之间的细小差异及扫描天顶角不同，使土壤的BRDF引起部分覆盖度反演误差。

从图3整个研究区的覆盖度反演结果统计来看，超过80%的像元反演值在实测值的分布范围内，这与同一地区同一农作物长势相近的实际相符，异常值可以看作是分类结果引起的，马路等的覆盖度几乎为0，而当时的小麦和果园等覆盖度都高于玉米。

4.2 反演LAI

玉米叶子分布一般认为是球形分布，取先验知识G=0.5，同时Nilson参数是一个与观测天顶角、行播作物的垄宽、垄距、冠层高度及叶面积指数等有关系的变量，根据实测的玉米几何结构参数，利用闫彬彦等人的方法估算Nilson参数随观测天顶角角度的变化关系(闫彬彦 等，2010)，如图4所示。根据各子样区的孔隙率、激光扫描入射天顶角和尼尔逊参数，利用式(11)反演各子样区的LAI。对所有地块，各子样区LAI求均值，得到各地块反演的LAI(图5)。表2是反演LAI与实测LAI的比较，图6是整个研究区(整条航带)LAI反演结果的统计，图中的黑线表示实测LAI值的分布范围。

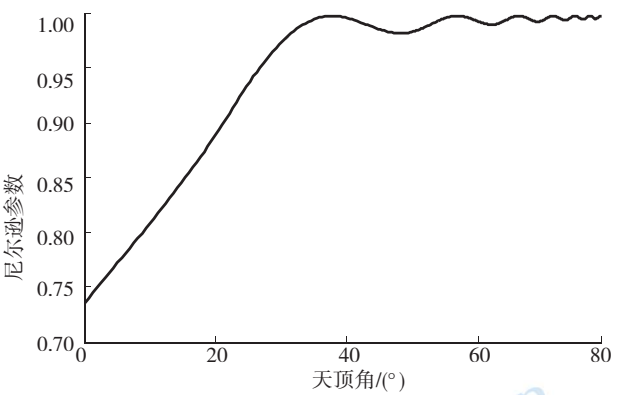

图4 尼尔逊参数随观测天顶角的变化图

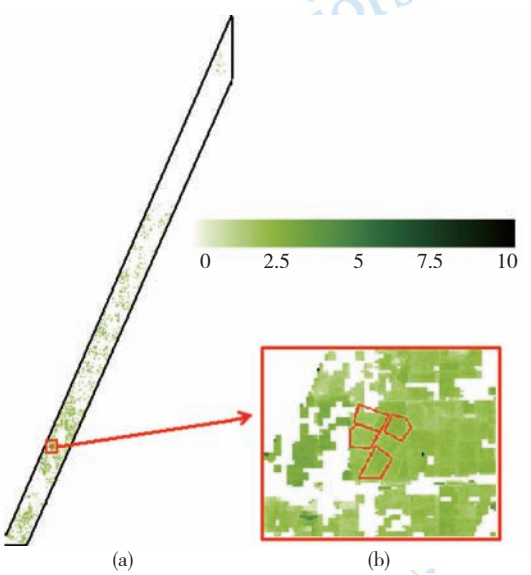

图5 Lidar反演的玉米LAI
(a) 整个研究区；(b) 验证区的4块样地

表2 玉米LAI反演值与实测值的比较

样地编号	Lidar反演结果		实测结果		绝对误差	相对误差/%
	均值	标准差	均值	标准差		
1	2.49	0.25	2.295	0.518	0.195	8.5
2	2.34	0.24	2.04	0.249	0.3	14.7
3	1.92	0.68	1.98	0.345	0.06	3
4	2.15	0.21	2.3	0	0.15	6.5

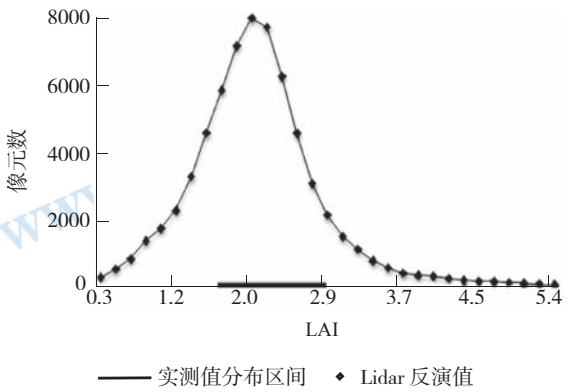

图6 整个研究区玉米LAI反演结果统计

从表2可以看出，Lidar的LAI反演结果与实测的LAI值相比总体上很接近，只有第2块地误差较大。误差产生的原因：LAI反演误差与覆盖度及Nilson参数有关，覆盖度的误差会部分地传递过来。Nilson参数与行播作物的垄向、*G*函数、垄宽、垄距、作物的冠层高度、叶面积指数及飞行方向等多种因素有关，本文采用的Nilson参数值是根据实地测量值的平均值来模拟的，Nilson参数随视角变化，尽管可以减少视角变化的影响，但Nilson参数带来的误差仍然不可避免。实际上，正如图4所示，对于行播作物而言，角度是影响Nilson参数的一个重要因素，在其他因素相同的情况下，考虑角度的Nilson参数更接近于真实的Nilson参数。因此本文所用方法与传统上使用Nilson参数时取一个固定值，完全不考虑视角对Nilson参数的影响相比，使LAI反演结果更接近于真实情况。

从图6的LAI反演结果的整体统计结果来看，研究区玉米LAI超过80%像元的LAI值都在实测范围之内，排除分类结果误差，符合一个地区农作物长势相似但不同的实际情况。

5 结 论

综合了激光雷达离散回波数据和全波形数据的特点，结合雷达方程，利用地面回波点数据，提出了针对低矮农作物的、基于强度的植被覆盖度反演方法，并以此为理论基础反演了整条航带的玉米覆盖度和LAI，实验验证表明这些方法切实可行。

Lidar数据的分类一直是一个较难解决的问题，而本文方法对农田特别是玉米地的Lidar点云数据分类有着较高的精度要求。本文首先采用DSM与DEM获取冠层高度模型，在此基础上结合同时期的可见光图像分类结果进行滤波处理，以较高精度提取了玉米Lidar点云数据。

本文以玉米为主要研究对象，反演了覆盖度和LAI，所用的方法是针对低矮植被提出的，对其他农作物和低矮植被适用。反演结果表明，利用Lidar数据能反演精确且分辨率高的农作物覆盖度和LAI。相信在未来对农田监测要求更高的农业生产方面(如精细农业等)，Lidàr有广泛的应用前景。

REFERENCES

Andersen H E, McGaughey R J and Reutebuch S E. 2005. Estimating forest canopy fuel parameters using LiDAR data. *Remote Sensing of Environment*, **94**(4): 441–449

Avissar R and Pielke R A. 1989. A parameterization of heterogeneous land surfaces for atmospheric numerical models and its impact on regional meteorology. *Monthly Weather Review*, **117**(10): 2113–2136 DOI: 10.1175/1520–0493(1989)117<2113:APOHLS>2.0.CO;2

Bao Y F, Cao C X, Zhang H, Chen E X, He Q S, Huang H B, Li Z Y, Li XW and Gong P. 2008. Synchronous estimation of DTM and fractional vegetation cover in forested area from airborne LIDAR height and intensity data. *Science in China Series E-Technological Sciences*, **51**(Suppl. 2): 176–187

Bonan G B. 1993. Importance of leaf area index and forest type when estimating photosynthesis in boreal forests. *Remote Sensing of Environment*, **43**(3): 303–314

Cohen W B, Maiersperger T K, Gower S T and Turner D P. 2003. An improved strategy for regression of biophysical variables and Landsat ETM+data. *Remote Sensing of Environment*, **84**(4): 561–571

Colombo R, Bellingeri D, Fasolini D and Marino C M. 2003. Retrieval of leaf area index in different vegetation types using high resolution satellite data. *Remote Sensing of Environment*, **86**(1): 120–131

Donoghue D N M, Watt P J, Cox N J and Wilson J. 2007. Remote sensing of species mixtures in conifer Remote sensing of species mixtures in conifer plantations using LiDAR height and intensity data. *Remote Sensing of Environment*, **110**(4): 509–522 DOI: 10.1016/j.rse.2007.02.032

Fan W J and Xu X R. 2005. Integrative inversion of land surface component temperature. *Science in China Series D-Earth Sciences*, **48**(11): 2011–2019

Guan F X and Li F W. 2009. Research on features extraction based on LiDAR. *Geomatics and Spatial Infromation Technology*, **32**(1): 134–135, 140

He Q S, Chen E X, Cao C X, Liu Q W and Pang Y. 2009. A study of Forest Parameters Mapping Technique using Airborne LIDAR Data. *Advances in Earth Science*, **24**(7): 748–755

Kotz B, Schaepman M, Morsdorf F, Bowyer P, Itten K and Allgower B. 2004. Radiative transfer modeling within a heterogeneous

canopy for estimation of forest fire fuel properties. *Remote Sensing of Environment*, **92**(3): 332–344

Langford J, Niemann O, Frazer G, Wulder M A and Nelson T. 2006. Exploring small footprint Lidar intensity data in a forested environment//*Proceedings*, *IEEE International Conference on Geoscience and Remote Sensing Symposium*. Denver: IEEE: 2416—2419

Lefsky M A, Cohen W B, Acker S A, Parker G G, Spies T A and Harding D. 1999. LiDAR remote sensing of the canopy structure and biophysical properties of Douglas-fir western hemlock forests. *Remote Sensing of Environment*, **70**(3): 339–361

Li Q and Ma H C. 2008. The study of Point-cloud Production Method based on Waveform Laser Scanner Data. *Acta Geodaetica et Cartographica Sinica*, **37**(3): 349–354

Means J E, Acker S A, Harding D J, Blair J B, Lefsky M A, Cohen W B, Harmon M E and McKee W A. 1999. Use of large-footprint scanning airborne lidar to estimate forest stand characteristics in the Western Cascades of Oregon. *Remote Sensing of Environment*, **67**(3): 298–308

Morsdorf F, Kötz B, Meier E, Itten K I and Allgöwer B. 2006. Estimation of LAI and fractional cover from small footprint airborne laser scanning data based on gap fraction. *Remote Sensing of Environment*, **104**(1): 50–61 DOI: 10.1016/j.rse.2006.04.019

Sasaki T, Imanishi J, Ioki K, Morimoto Y and Kitada K. 2008. Estimation of leaf area index and canopy openness in broad-leaved forest using an airborne laser scanner in comparison with high-resolution near-infrared digital photography. *Landscape and Ecological Engineering*, **4**(1): 47–55 DOI: 10.1007/s11355-008-0041-8

Schlerf M and Atzberger C. 2006. Inversion of a forest reflectance model to estimate structural canopy variables from hyperspectral remote sensing data. *Remote Sensing of Environment*, **100**(3): 281–294

Solberg S, Brunner A, Hanssen K H, Lange H, Naesset E, Rautiainen M and Stenberg P. 2009. Mapping LAI in a Norway spruce forest using airborne laser scanning. *Remote Sensing of Environment*, **113**(11): 2317–23271 DOI: 10.1016/j.rse.2009.06.010

Sui L C and Zhang B Y. 2006. Principle and trend of Airborne Laser Scanning Remote Sensing. *Journal of Zhengzhou Institute of Surveying and Mapping*, **23**(2): 127–129

Wagner W, Ullrich A, Ducic V, Melzer T and Studnicka N. 2006. Gaussian decomposition and calibration of a novel small-footprint full-waveform digitising airborne laser scanner. *ISPRS Journal of Photogrammetry and Remote Sensing*, **60**(2): 100–112 DOI: 10.1016/j.isprsjprs.2005.12.001

Weiss M and Baret F. 1999. Evaluation of canopy biophysical variable retrieval performances from the accumulation of large swath satellite data. *Remote Sensing of Environment*, **70**(3): 293–306 DOI: 10.1016/S0034-4257(99)00045-0

Yan B Y, Xu X R and Fan W J. 2010. A unified canopy bidirectional reflectance(BRDF) model for row crops. *Science in Chnia Series D*, Accepted

Yao Y J, Fan W J, Liu Q, Li L, Tao X, Xin X Z and Liu Q H. 2010. Improved harvesting method for corn LAI measurement in corn whole growth stages. *Transactions of the CSAE*, **26**(8): 189–194

Zhao K G and Popescu S. 2009. LiDAR-based mapping of leaf area index and its use for validating GLOBCARBON satellite LAI product in a temperate forest of the southern USA. *Remote Sensing of Environment*, **113**(8): 1628–1645

Zhang J, Zhang X Y and Cao H C. 2009. Post-processing of Airborne LiDAR Data based on Terrasolid Software. *Sci-Tech Information Development and Economy*, **19**(26): 90–92

附中文参考文献

关辅兴，李芳伟．2009．LiDAR地物提取研究．测绘与空间地理信息，**32**(1): 134–135, 140

何祺胜，陈尔学，曹春香，刘清旺，庞勇．2009．基于LiDAR数据的森林参数反演方法研究．地球科学进展，**24**(7): 748–755

李奇，马洪超．2008．基于激光雷达波形数据的点云生产．测绘学报，**37**(3): 349–354

隋立春，张宝印．2006．Lidar遥感基本原理及其发展．测绘科学技术学报，**23**(2): 127–129

闫彬彦，徐希孺，范闻捷．2010．行播作物二向性反射(BRDF)的一体化模型．中国科学D辑(接收)

姚延娟，范闻捷，刘强，李丽，陶欣，辛晓洲，柳钦火．2010．玉米全生长期叶面积指数收获测量法的改进研究．农业工程学报，**26**(8): 189–194(请调整本条文献顺序)

张娟，张小叶，曹海春．2009．基于Terrasolid系列软件的机载LiDAR数据后处理．科技情报开发与经济，**19**(26): 90–92